# Evidence of trivalent Am substitution into U3O8

Caisso, M.; Roussel, P.; Den Auwer, C.; Picart, S.; Hennig, C.; Scheinost, A. C.; Delahaye, T.; Ayral, A.;

Originally published:

September 2016

**Inorganic Chemistry 55(2016), 10438-10444**

DOI: https://doi.org/10.1021/acs.inorgchem.6b01672

# Evidence of trivalent Am substitution into $U_3O_8$

*Marie Caisso[1,2,7], Pascal Roussel[3], Christophe Den Auwer[4], Sébastien Picart[2], Christoph Hennig[5], Andreas C. Scheinost[5,6], Thibaud Delahaye[2,*], André Ayral[7]*

[1]CEA, DEN, DTEC/SECA/LFC, F-30207 Bagnols-sur-Cèze Cedex, France

[2]CEA, DEN, DRCP/SERA/LCAR, F-30207 Bagnols-sur-Cèze Cedex, France

[3]Unité de Catalyse et Chimie du Solide, UMR 8012 CNRS, 59652 Villeneuve d'Ascq Cedex, France

[4] Université Nice Sophia Antipolis, Institut de Chimie de Nice, UMR 7272, F-06108 Nice cedex 2

[5]HZDR, Institute of Resource Ecology - 01314 Dresden, Germany

[6]The Rossendorf Beamline at ESRF – 38043 Grenoble, France

[7]Institut Européen des Membranes, UMR 5635 CNRS-ENSCM-UM2, CC047, Université Montpellier 2, F-34095 Montpellier Cedex 5, France

KEYWORDS. $U_3O_8$, uranium-americium mixed oxide, EXAFS, XANES, XRD.

ABSTRACT. $U_3O_8$ is considered as the most stable phase for uranium oxide, justifying the necessity to precisely know its structural properties in order to apprehend its behavior in storage conditions as regards leaching in the case of spent nuclear fuel storage in oxidative conditions.

Nevertheless, as fuel irradiation causes the formation of fission products and activation products such as plutonium and minor actinides, it is probable that $U_3O_8$ oxide would be mixed with other chemical elements in real conditions of oxidation. Storage issue can be extended to americium transmutation where compounds dedicated to irradiation are mixed-oxides composed of uranium and americium. Present study is thus focusing on the determination of the structural properties of a solid solution containing uranium and trivalent americium (U/Am ratio = 90/10), and synthetized as to obtain conventional $U_3O_8$ oxide. It presents for the first time the possibility to combine trivalent americium with uranium as mixed-oxide under $U_3O_8$ form, despite the high valence and atomic ratio differences, and propose novel structural arrangements. XRD measurements reveal americium substitution in $U_3O_8$ uranium cationic site, leading to phase transformation to $U_3O_8$ high temperature structure and general lattice swelling. XANES and EXAFS experiments highlight, as main consequence for accommodation, excess of $U^{+VI}$ organized in uranyl units.

## INTRODUCTION

Oxidation of uranium (U) dioxide ($UO_2$) into $U_3O_8$ has been studied for years in the field of nuclear fuel fabrication. It was first considered for nuclear fuel reprocessing, and is now considered in waste management domain and spent fuel behavior in dry storage conditions.[1,2] Indeed, as $UO_2$ is the most common uranium form used as nuclear fuel, $U_3O_8$ is the most stable uranium oxide in ambient conditions, close to the U compounds found in natural environment. Left at room temperature (RT) under air, $UO_2$ is slowly oxidized into $U_3O_8$.[3] Focusing on spent fuels, even if major part is still composed of $UO_2$, the presence of additional radionuclides with high radioactivity such as fission products or minor actinides (MA) and thus generating heat

load, leads to faster $UO_2$ oxidation into $U_3O_8$, accelerating intermediate phase transformation such as $U_4O_9$ and $U_3O_7$.[4] This issue also concern compounds fabricated in the field of MA transmutation,[5,6] where the latter can be integrated to uranium oxides, to form, in the case of americium (Am), dense $U_{1-x}Am_xO_{2\pm\delta}$ pellets. Storage and post-irradiation behavior of these compounds under oxidative conditions remain unknown and are identified as crucial factors for future experimental irradiation. Furthermore $U_3O_8$ compound is also used as mineral poreformer in nuclear fuel fabrication.[7,6] Impurity solubility in this oxide should thus be well-known to anticipate chemical reaction between $U_3O_8$ as poreformer and other actinides composing fuels, such as MOX fuel[8,9] or dedicated compounds for transmutation.

Considering first literature on pure $U_3O_8$, at RT its crystalline structure was determined as orthorhombic (space group *C2mm*) and this form is called α-$U_3O_8$.[10–13] When heated at 483 K, α form is converted into α' one with transition to hexagonal space group *P-62m*. This transition and the consequent atomic positions modifications were studied by Loopstra et al.[14] and Ackermann et al.[15], who defined current space group and positions for U and O in α-$U_3O_8$ and α'-$U_3O_8$ forms. If many characterizations have been performed on $U_3O_8$ to explain crystallographic structures,[10,12,14,16,17] few papers exist on $U_3O_8$ accommodating with another chemical element. Tetravalent Pu and Np were integrated to $U_3O_8$ to form a solid solution. Benedict et al. report some space group change with Pu incorporation,[18] such as Finch et al. for Np,[19] but no structural models were presented to explain how these elements present as impurities are accommodated in the structure. More recently, Remy synthetized same kind of mixed oxide containing tetravalent Ce.[20] In the following study, Am was the chosen substituted element, answering transmutation target research need for post-irradiation characterizations. Mixed oxides composed of U and Am were synthetized under oxidative atmosphere, in the same conditions required for $U_3O_8$

formation.[21–23] Obtained crystalline structure was fully characterized and compared to pure $U_3O_8$. To begin, XRD results presenting the new crystalline structure and its difference with the pure compound are exposed and analyzed. These results were completed by XANES measurements allowing to assess the formal oxidation states of U and Am in the mixed-oxide. Finally EXAFS data fitting was used to reconstruct the close environment of the U and Am cations and the establishing of metal-O and metal-metal first distances, highlighting what enables Am to be substituted in the $U_3O_8$ structure.

## EXPERIMENTAL SECTION

**Sample preparation.** A wet chemical route based on the use on ion exchange resin microspheres was selected in this work to ensure in the final oxide a homogeneous repartition of actinide element at the atomic scale. This process of (U,Am) based samples was the same as described in previous works for actinide based mixed-oxide synthesis.[22,23] Stoichiometric amounts of uranyl and americium cations dissolved in aqueous solution, implying the following atomic U/Am ratio of 90/10, were fixed on the exchanger sites of weak acid resin (WAR) microspheres, releasing proton ions. After complete exchange (stable pH of the solution), loaded resin was extracted and dried at 373 K. Microspheres were finally calcined for 4 h at 973 K under air, following a heating rate of 5 $K.min^{-1}$. This calcination was performed in a tubular furnace (Lenton LTF), in which microspheres were disposed as a single layer in a quartz crucible. The same protocol was followed for pure $U_3O_8$ reference microspheres.

**X-Ray Diffraction.** RT XRD diagrams were recorded on powdered microspheres using a Bruker D8 Advance apparatus equipped with a Cu Kα1,2 radiation and a linear Lynx-Eye detector, in a θ-θ Bragg–Brentano configuration. The step was approximately fixed at 0.02° with

a time per step of 0.3 s, for an angular domain of 15 to 110° 2θ. Bruker EVA DIFFRACplus software was used for phase identification. Lattice parameters of synthesized compounds were determined using the Jana Suite software,[24,25] with a Le Bail method for refinements.[26] A pseudo-Voigt profile function was used for lattice parameter refinement. Gold reference was added to the powdered sample for position calibrations. The Au phase profile was also fitted but lattice parameters were kept fixed as it is used as a reference.

**XAS experiments.** XAS experiments were carried out at the European Synchrotron Radiation Facility (ESRF, Grenoble, France) on the Rossendorf Beamline (ROBL) with the storage ring operating at 6.0 GeV and 170−200 mA. The synchrotron beam was collimated with a 1.3 m long, Rh-coated, meridionally-bent mirror, monochromatized with a double-crystal monochromator with a water-cooled Si (111) crystal pair, and focalized with a 1.2 long, Rh-coated toroidal mirror. XANES spectra were collected in transmission mode at the Am $L_{III}$ (18510 eV) and the U $L_{III}$ edge (17166 eV) with a step size of 0.7 eV using ionization chambers. EXAFS measurements were performed in both transmission and fluorescence modes, at the Am $L_{III}$ (18510 eV) and U $L_{II}$ (20948 eV) edges for Am-substituted $U_3O_8$ microspheres, and U $L_{III}$ edge for pure $U_3O_8$ microspheres. The use of the U $L_{II}$ edge was necessary because of the presence of neptunium impurities in Am, with its $L_{III}$ absorption edge interfering with the U $L_{III}$ EXAFS region. The fluorescence signal was measured with a 13-element Ge solid-state detector using a digital spectrometer (XIA-XMap). Metallic foils whith K edges close to the edges of interest, i.e. Y (17038 eV), Zr (17998 eV), and Mo (20000 eV), were used as references for energy calibration. EXAFS spectra were recorded at Am $L_{III}$, U $L_{II}$ and U $L_{III}$ edges, up to k = 18, 13.5 and 16 $Å^{-1}$, respectively. During all the measurements, a He cryostat was used to maintain a sample temperature around 15 K. The thermal contribution to the Debye-Waller factors is thus

greatly reduced and only the static structural disorder contribution remains. Data refinements were performed using the IFEFFIT[27,28] software and FEFF9[29] for ab initio calculations of EXAFS spectra. XANES spectra were normalized using a linear function for pre- and post-edge approximation. $E_0$ was arbitrarily assigned to the edge inflection point, determined as the knot of the first derivative. U $L_{III}$ edge spectra were compared to that of a $UO_3$ compound also recorded at ROBL under the same conditions, while the Am $L_{III}$ spectra were compared to those of $AmO_2$ and pure Am oxalate,[30] as $Am^{+IV}$ and $Am^{+III}$ references respectively. Considering the pure $U_3O_8$ reference, Fourier transform of the EXAFS spectrum (in $k^2$) was performed with a Hanning window between 2.2 and 16 $Å^{-1}$. For the Am-substituted $U_3O_8$, Fourier transform of the EXAFS spectra (in $k^2$) was performed with a Hanning window between 3 and 13 $Å^{-1}$ and 3.5 and 2.8 and 11.8 $Å^{-1}$ for U $L_{II}$ and Am $L_{III}$ edges respectively. A 7.5 Å-cluster of $U_3O_8$ was considered for data fitting, using the lattice parameters determined through XRD measurements. Model $U_3O_8$ was fitted with C2mm space group. In this crystallographic structure, U is coordinated by two axial O, 5 equatorial O, 2 axial U and 4 equatorial U as nearest neighbors. Multiple scattering along axial directions was taken into account through the addition of triple scattering ($U_1$-$O_2$-$O_X$-$U_1$) and quadruple scattering ($U_1$-$O_2$-$U_X$-$O_2$-$U_1$). The structural parameters of the multiple scattering paths were linked to that of corresponding single scattering paths to reduce the number of free parameters. Considering Am-substituted $U_3O_8$, two space groups were tested, *P-3m1* and *P-62m*, but only the latter allowed the fit to converge. For *P-62m*, the configuration of single scatterings around U is the same as for *C2mm* with a few changes on distances. Consequently similar triple and quadruple scattering paths were also added and improved the fit quality, with structural parameters linked to the single paths. Debye-Weller factors were found equal to 0.005(1) and 0.0080 $Å^2$, and 0.0200 and 0.0150 $Å^2$ for $UL_{II}$ and $AmL_{III}$ edges respectively.

## RESULTS AND DISCUSSION

The following results present and develop the features of the crystallographic structure obtained after (U,Am) loaded resin thermal conversion under air, performed at 973 K. These novel features are compared to pure $U_3O_8$ microspheres.

**XRD results.** XRD recorded diagrams for pure $U_3O_8$ and Am-based $U_3O_8$ microspheres are presented in Figure 1 and Figure 2 respectively. For pure $U_3O_8$ X-Ray phase diagram, phase identification matches with the orthorhombic *C2mm* crystallographic structure. In the context of uranium oxides, it corresponds to the α-$U_3O_8$ phase, structure stabilized at RT. Le Bail refinement performed on this recorded diagram gives the following lattice parameters: a = 6.720(2) Å; b = 11.952(2) Å; c = 4.146(2) Å for a lattice volume of 333.02(1) $Å^3$. Refinement parameters are summarized in Table 2 and corresponding plots are presented in Figure 1. Structural values, when compared to literature,[12,14,15] are relevant of standard α-$U_3O_8$ phase and validates the synthesis of $U_3O_8$ compound through thermal conversion of WAR microspheres under air at 973 K.

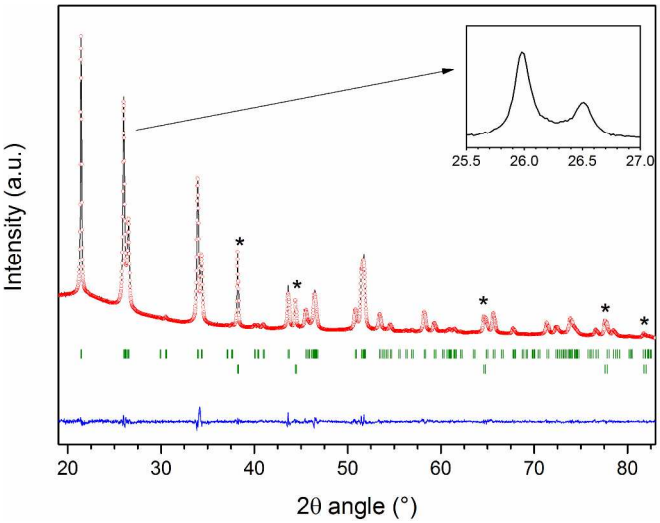


Figure 1. XRD diagram and refinement results of powdered pure $U_3O_8$ oxide microspheres converted during 4h at 973 K under air – Peak matches with a * correspond to gold phase.

Experimental data is in black; the calculated diagram is in red; the difference between them is in blue; Bragg positions are presented in green.

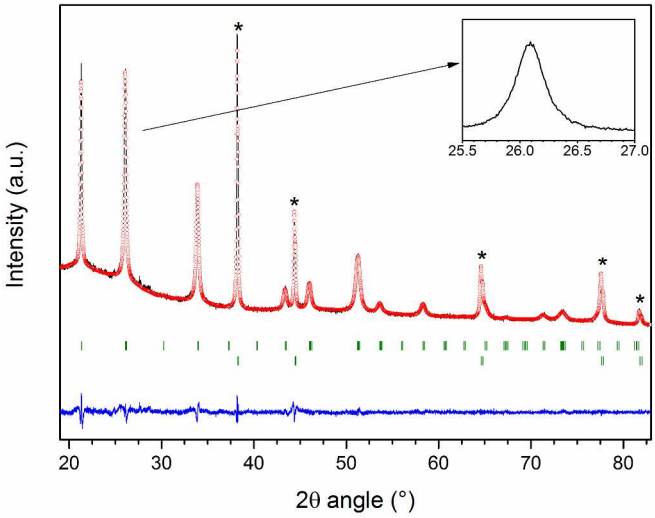


Figure 2. XRD diagram and refinement results of (U,Am) based oxide microspheres converted during 4h at 973 K under air – Peak matches with a * correspond to gold phase. Experimental data is in black; the calculated diagram is in red for P-62m reference space group; the difference between them is in blue; Bragg positions are presented in green.

Considering X-Ray diagram collected after thermal conversion of WAR microspheres loaded with U and Am, Figure 2, a diagram associated to a monophasic compound is also obtained after conversion, but if it looks close to that α-$U_3O_8$ phase, a relevant difference is noticed on the two peaks around 26.5° (enclosed zoom) and 34°. Indeed, pure $U_3O_8$ phase shows two significant peaks that become merged into a single one in the new phase including Am. About phase identification, two crystallographic structures match with the collected diagram. The first one crystallizes in the trigonal *P-3m1* space group, taken by α-$UO_3$ phase,[31] and the second one in the hexagonal *P-62m* space group, stabilized at HT (over 500 K) by $U_3O_8$.[15] Both own similar cationic sublattice with single cationic position, where differences are undertaken by the O

atoms. In the case of trigonal structure, there are only two O positions, for five positions in hexagonal one, consistent with higher anionic organization in the case of hexagonal structure. The adjustment of crystalline structure with Am presence, through this change of space group, is relevant of Am substitution inside $U_3O_8$ phase. Le Bail refinements were performed for both possibilities. The lattice parameters determined for *P-62m* space group, whose refinement is visible in Figure 2, are: a = 6.838(2) Å; c = 4.171(2) Å for a total lattice volume of 169.05(1) Å$^3$. When refined with *P-3m1* space group, the following lattice parameters were obtained: a = 3.948(2) Å and c = 4.167(2) Å for a total lattice volume of 56.33(1) Å$^3$, where a factor of the trigonal structure is found equaled to a of hexagonal one divided by $\sqrt{3}$. If comparing now normalized volume of each crystalline structure (Table 1), a relevant swelling of the structure clearly appears for the sample containing Am. The global increase is close to 5 Å$^3$, which is a significant value for lattice modification that confirms the substitution of Am on U site in $U_3O_8$ oxide.

Table 1. Summarize of the calculated lattice volume for pure $U_3O_8$ and Am-substituted $U_3O_8$.

| | **Pure $U_3O_8$** | **Am-substituted $U_3O_8$** | |
|---|---|---|---|
| Space group | *C2mm* | *P-62m* | *P-3m1* |
| Volume (Å$^3$) | 333.02(2) | 169.05(2) | 56.33(2) |
| Normalized volume (Å$^3$) | 333.02(2) | 338.10(2) | 337.98(2) |

Table 2. Fit parameters obtained after LeBail refinement of the two studied samples.

| **Phase** | **Pure $U_3O_8$** | **Am-substituted $U_3O_8$** | |
|---|---|---|---|
| Space group | *C2mm* | *P-62m* | *P-3m1* |
| GOF | 1.44 | 1.30 | 1.50 |
| $R_p$ | 2.54 | 2.79 | 2.82 |
| $wR_p$ | 3.48 | 3.60 | 3.74 |

**XAS results.**

*XANES.*

The spectra recorded at the Am $L_{III}$ edge for Am-substituted $U_3O_8$ and model compounds are presented in Figure 3. The comparison between the sample spectrum and the reference for $Am^{+IV}$ and $Am^{+III}$ clearly shows that Am is totally trivalent in the Am-substituted $U_3O_8$ structure. Concerning the corresponding U $L_{III}$ edge, spectra (and corresponding derivatives) recorded for pure α-$U_3O_8$, $UO_3$ and Am-substituted $U_3O_8$ are presented in Figure 4. $UO_3$ corresponds to pure $U^{+VI}$ cation ("yl" like), illustrated by two distinct bands after absorption edge in Figure 4, relevant of two distant U-O distances present: 2.1 Å for apical distance and around 2.38 Å for equatorial distances.[32,33] For α-$U_3O_8$ reference, spectrum presents a single significant band after absorption edge, characteristic of the *C2mm* crystallographic structure with similar U-O. The valence of U in $UO_3$ is +VI while $U_3O_8$ presents two different U oxidation states (+V and +VI) in order to guarantee the electroneutrality inside the oxide.[34] Considering $U_3O_8$ as stoichiometric oxide at RT, U element is distributed for 33% in $U^{+VI}$ and 66% in $U^{+V}$ for an average valence of 5.33.

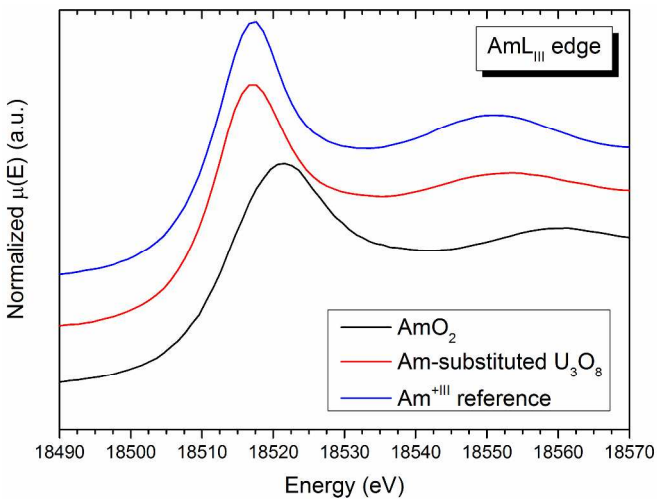


Figure 3. Normalized XANES spectra collected at Am $L_{III}$ edge and 20 K – $AmO_2$ is in dark grey, Am-substituted $U_3O_8$ is in blue and the $Am^{+III}$ reference is in red.

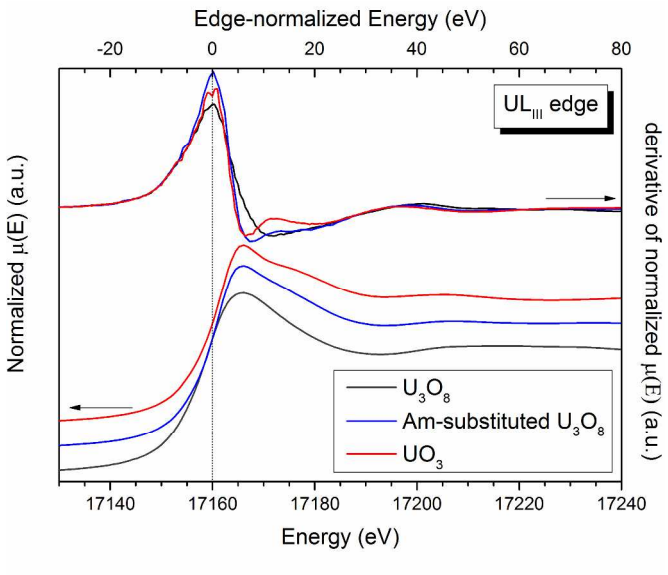


Figure 4. Normalized XANES spectra collected at U $L_{III}$ edge and associated derivatives. 20 K – $U_3O_8$ is in dark grey, Am-substituted $U_3O_8$ is in blue and $UO_3$ is in red.

When looking at Am-substituted $U_3O_8$ spectrum, it looks intermediary between the two pure uranium oxides. Although it is not as pronounced as for $UO_3$, two bands are present on the absorption derivative after absorption edge, illustrated by a small shoulder around 17180 eV,

which is completely absent of the $U_3O_8$ spectrum. This observation would thus be consistent with the presence of two different U-O distances in (U,Am)-based oxide approaching the "yl" like configuration (as in $UO_3$). Indeed Figure 4 suggests that U lies in a mixed-valence state with unknown +V/+VI. Only high resolution XANES would allow to precisely confirm mixed-valence and quantitative proportion of +V and +VI. Indeed, the resolution of the core hole at the An $L_{II,III}$ edge (around 7 eV) is far too small to enable such determination with accuracy. One can conclude that Am-substituted $U_3O_8$ XANES derivative (post edge shape) is thus qualitatively closer from that of $UO_3$ than from $U_3O_8$. If considering 10 at%. of trivalent Am on +V/VI U sites, average U charge for stoichiometric oxide will shift from 5.33 (for pure $U_3O_8$) to 5.59. This would correspond to the presence of 60% of $U^{+VI}$ in the mixed oxide instead of 33% in pure $U_3O_8$, to compensate trivalent Am presence.

Considering XRD results, previous work validates the hypothesis of substitution, thanks to the observed change of crystallographic structures from pure $U_3O_8$ to Am-substituted $U_3O_8$. Knowing the oxidation state of Am in the sample (+III), comparison can be made between the sizes of the different cations in presence. Considering ionic radius of trivalent Am in hexaedral environment equals 1.115 Å for 0.87 Å for $U^{+VI}$ and 0.9 Å for $U^{+V}$,[35] it helps to explain the global increase of lattice volume with Am-substituted $U_3O_8$ visible in Table 1.

EXAFS study was also performed in order to better understand how the crystalline structure accommodates the presence of trivalent Am, what are the close environment of U and Am, and what are the differences compared to pure $U_3O_8$. This will thus help to confirm possible formation of "yl" units.

EXAFS.

k²-weighed EXAFS spectrum and corresponding Fourier transform of pure $U_3O_8$ are presented in Figure 5 and Figure 6. The best fit structural parameters are summarized in Table 3. For this *C2mm* model structure, fitted distances for single paths are close to crystallographic data. Concerning the first U-O axial path, uncertainty is high and the corresponding Debye-Weller factor exhibits a quite high value (0.03 Å²). This is due to complicated signal extraction at low k range for this kind of oxides, resulting in large Debye-Waller factors, and high uncertainties for the first shell. Nevertheless, the other distances confirm the correspondence with *C2mm* space group defined for pure α-$U_3O_8$, particularly through sub-cationic lattice and U...U interatomic distances that were fitted until 5.6 Å.

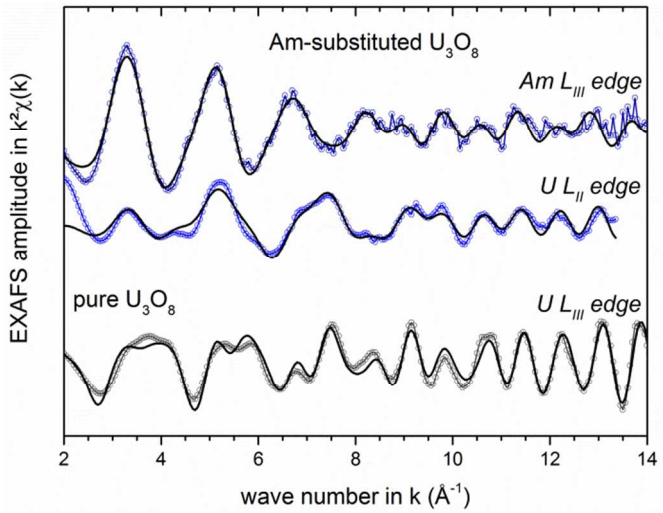


Figure 5. k²-weighted EXAFS spectra of the pure $U_3O_8$ and Am-substituted $U_3O_8$. Experimental spectra are plotted in dots (dark grey: pure $U_3O_8$ at U $L_{III}$ edge; blue and light blue: Am-substituted $U_3O_8$ at $UL_{II}$ and $AmL_{III}$ edges respectively, adjustments in black lines.

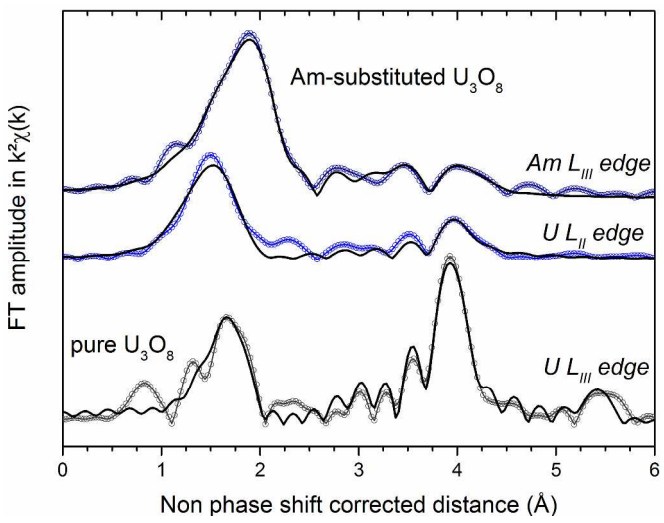


Figure 6. Fourier transform of the EXAFS spectra for pure $U_3O_8$ and Am-substituted $U_3O_8$. Experimental spectra are plotted in dots (dark grey: pure $U_3O_8$ at U $L_{III}$ edge; blue and light blue: Am-substituted $U_3O_8$ at $UL_{II}$ and $AmL_{III}$ edges respectively, adjustments in black lines.

Considering Am-substituted $U_3O_8$, both *P-3m1* and *P-62m* space groups were first tested as model references for fitting at the U edge. The trigonal structure did not show good correlation between experimental plot and fit, tending to assess that metal-O and metal…U distances in the sample are closer to the ones identified in the hexagonal reference configuration. Therefore as a starting point for fitting, the path lengths in *P-62m* structure were considered as model for both Am and U edges.

Focusing on Am environment, Table 3 presents the best fit parameters. XRD previously showed the substitution of Am on U site. Good results obtained for EXAFS spectrum fitting tends to confirm these results, as Am-O and Am…U distances are in good agreement with the ones corresponding to *P-62m* structure. The increase of interatomic Am-O distances is in agreement with the decrease of formal oxidation state from +5.33 for U in $U_3O_8$ *C2mm* to +3 for Am in the present structure, although this is only indicative because both cations don't have the same geometry. Moreover, as $Am^{+III}$ has a larger crystal radius (1.115 Å) than U in the same

hexahedral configuration (0.87 Å for $U^{+VI}$ and 0.9 Å for $U^{+V}$),[35] it should also contribute to the expansion of the O environment. The fit of the Am...U distances was only possible if considering an important shortening of the four equatorial Am-U paths, whereas axial distances increase. This significant variation, opposing the general tendency of swelling, can be understood if anionic and cationic paths are de-correlated. This can be assumed as anionic interatomic distances undergo different variations from cationic sublattice, and cations and anions are not aligned together on the same direction. It thus renders possible Am…U equatorial distance shrinkage, despite swelling of anionic sublattice. On contrary, for the axial direction where Am and O are aligned, both Am-O and Am…Am distances increase.

Fitting U $L_{II}$ EXAFS spectrum for Am-substituted $U_3O_8$ evidences several structural modifications of U closest environment compared to the *P-62m* structure, summarized in Table 3. Concerning the U-O single scattering, optimization of the fit led to a split of axial U-O distances into two different contributions, with a repartition close to 50/50. The first one equals 2.03(1) Å and remains very similar to the crystallographic value of 2.07 Å in *P-62m*. The second one is found significantly shorter than conventional distance in $U_3O_8$, and equals 1.78(1) Å. Tentative to remove this short distance or to compensate with a higher Debye Waller value for the first shell lead to a very significant degradation of the quality factor ($\Delta\chi^2\nu$ = 27 to 265). In addition, this result is correlated to the above discussion on XANES spectra, and suggests that 50(5) % of the U-O bond can be assimilated to "uranyl" as it is very close to uranyl theoretical distance (1.76 Å[36]). As a consequence one may assume that trivalent Am substitution in $U_3O_8$ induces structural and charge modifications with an increase of $U^{+VI}$, as expected with previous calculation of charge compensation leading to 60% of $U^{+VI}$ required, instead of 33%. Excess of +VI cation thus needs to be organized in the structure through the formation of “uranyl” like

units observed by XANES and fitted by EXAFS. Concerning the equatorial U-O distances, values determined for the five paths are in agreement with the *P-62m* model: 2.16(1) Å compared to 2.21 Å for the four symmetric surrounding O, and 2.62(1) Å compared to 2.67 Å for the single one. Focusing now on cationic sublattice, the U...U interatomic distance also reveals important modifications with important increase of one distance (+0.16 Å), linked to the four equatorial U...U paths, whereas simple axial interatomic distances remain close to crystallography. Addition of triple and quadruple scattering paths linked to 2.07 Å U-O axial distances considerably improved the quality of the fit. This result strengthens the assumption of the coexistence of free uranyl like bonds together with normal U-O axial bonds linked to the sub-cationic lattice.

The structural arrangements around U and Am, in pure $U_3O_8$ and in Am-substituted $U_3O_8$ are thus very different. According to the above data, the Am cation substitutes U and provokes general swelling of its close environment except for the Am…U equatorial distances that are decreased. The U and O atoms of the Am equatorial plane are not aligned, and make possible this Am…U distance modification. This is also evidenced by the U...U distortion caused by the presence of Am with different structural constraints on cationic and anionic sublattices. The major adjustment to the *P-62m* structure comes from the necessity to add to the system shorter free U-O bonds which would be related to axial uranyl like units, as illustrated in Figure 7. Scheme thus shows the two kinds of cationic and anionic environment around U and Am. The left part shows *P-62m* configuration taken by Am and 50% of U, mostly $U^{+V}$, besides distance distortion. Green atoms correspond to U or Am cations around absorbing cation, whereas red ones are O. The right configuration illustrates the environment determined with free “yle” units around U, attributed to $U^{+VI}$, identified with the two blue double U=O bonds. As a conclusion,

from U environment, anionic sublattice undergoes the major part of structural changes through free uranyl double bonds formation induced by a higher amount of $U^{+VI}$ in the mixed oxide, to compensate $Am^{+III}$ presence. As $U_3O_8$ oxides have planar disposition, this specific configuration enables to presume that it favors alternating uranyl planes with conventional $U^{+V}$ *P-62m* planes.

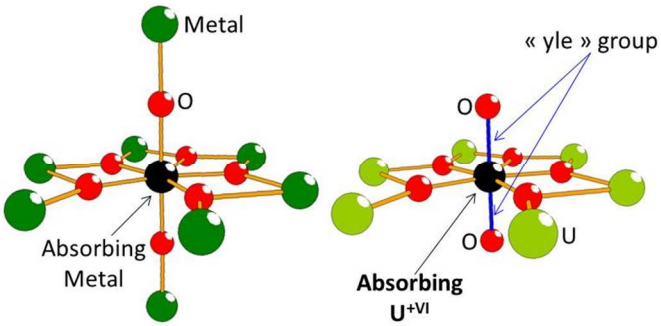


Figure 7. (left) First anionic and cationic coordination shells for *P-62m* space group used for EXAFS fitting. (right) First anionic and cationic coordination shells for $U^{+VI}$, involving "yle" configuration - Green atoms correspond to metals (U, Am), light green atoms to U, red ones to O. Black atom is considered as absorbing atom. Orange bond are simple and blue ones are double.

Table 3. EXAFS data on pure $U_3O_8$ and Am-substituted $U_3O_8$, and comparison with theory. $S_o^2$ is the EXAFS global amplitude factor, $\Delta e_0$ is the energy threshold, ε is the average noise and $R_{factor}$ is the agreement factor of the fit. Numbers in round brackets are uncertainties.

| | | Bond type | Distance (Å) | *crystallography ref (Å)* | $\sigma^2$ (Å$^2$) |
|---|---|---|---|---|---|
| **Pure $U_3O_8$ reference** *C2mm* | **U $L_{III}$ edge** $R_{factor}$ = 3.1% $\Delta\chi^2_\nu$ = 0.57 $S_0^2$ = 0.8 $\Delta e_0$ = 5.85 ε = 0.004 | 2 axial U-O | 1.99(5) | *2.07* | 0.0301 |
| | | 4 equatorial U-O | 2.21(1) | *2.16* | 0.0077 |
| | | 1 equatorial U-O | 2.59(1) | *2.54* | 0.0237 |
| | | 2 equatorial U...U | 3.70(1) | *3.74* | 0.0084 |
| | | 2 equatorial U...U | 3.84(1) | *3.88* | 0.0138 |
| | | 2 equatorial U...U | 4.14(1) | *4.18* | 0.0065 |
| | | 2 axial U...U | 4.16(1) | *4.15* | 0.0065 |
| | | 8 diagonal U...U | 5.62(1) | *5.59* | 0.0070 |
| **Am-substituted $U_3O_8$** | **U $L_{II}$ edge** $R_{factor}$ = 3.6% $\Delta\chi^2_\nu$ = 27.48 $S_0^2$ = 0.9 $\Delta e_0$ = -4.77 ε = 0.003 | (50%) 2 axial U-O | 2.03(1) | *2.07* | 0.0165 |
| | | (50%) 2 axial U=O' | 1.78(1) | *2.07* | 0.0036 |
| | | 4 equatorial U-O | 2.16(1) | *2.21* | 0.0085 |
| | | 1 equatorial U-O | 2.62(1) | *2.67* | 0.0159 |
| | | 6 equatorial U-U | 4.01(2) | *3.83* | 0.0137 |
| | | (50%) 2 axial U-U | 4.17(1) | *4.14* | 0.0015 |
| | **Am $L_{III}$ edge** $R_{factor}$ = 7.7% $\Delta\chi^2_\nu$ = 4.56 $S_0^2$ = 1.0 $\Delta e_0$ = 6.02 ε = 0.012 | 2 axial Am-O | 2.26(1) | *2.07* | 0.0033 |
| | | 4 equatorial Am-O | 2.46(2) | *2.21* | 0.0032 |
| | | 1 equatorial Am-O | 2.93(2) | *2.68* | 0.0022 |
| | | 6 equatorial Am-U | 3.69(2) | *3.83* | 0.0178 |
| | | 2 axial Am-U | 4.27(2) | *4.15* | 0.0028 |

## CONCLUSION

These experiments have investigated for the first time the possibility for trivalent Am to be substituted in α-$U_3O_8$ structure. Combination of XRD and XAS experiments led to the conclusion that substitution is possible thanks to structure accommodation, through transformation from initial orthorhombic to hexagonal structure for Am-substituted oxide. The latter, corresponding to *P-62m* space group, owns a single cationic site, increasing the global symmetry of the structure, but also attesting of a higher metallic disorder. The global cationic charge order of orthorhombic structure (*C2mm* space group), where $U^{+V}$ and $U^{+VI}$ get their own metallic site, is broken by the presence of trivalent Am, leading to space group change. Focusing on close environment of U and Am in the mixed-oxide determined through EXAFS analysis, Am is well-fitted with distances characteristic of hexagonal structure, but causes general increase of interatomic distances around it. U is suffering from more structural rearrangements with the formation of "yl" like bonds, resulting in structural re-organization of $U^{+VI}$ in uranyl units, whose quantity is increased to 60% instead of 33% to compensate trivalent Am presence. Planar geometry of $U_3O_8$-type oxides suggests alternating planes of $U^{+VI}$ with uranyl units, and $U^{+V}$ in conventional *P-62m* configuration. These results are first new insights on the possibility for $U_3O_8$ to accommodate, when submitted to high stress such as substitution of trivalent actinide, and propose first solutions for structural arrangements.

## AUTHOR INFORMATION

### Corresponding Author

* Dr. Thibaud Delahaye: thibaud.delahaye@cea.fr ; 0033466796542 – CEA, DEN, DRCP/SERA/LCAR, F-30207 Bagnols-sur-Cèze Cedex, France

ACKNOWLEDGMENT

The authors would like to thank F. Boucher for his precious advices on oxide structures. They also thank M. Bataille and P. Coste for sample preparation; A. Gauthé, I. Jobelin, P. Grangaud and J.-M. Pomarède for sample synthesis. We acknowledge the ESRF Synchrotron Light Source for provision of beamtime at the ROBL beamline and P. Colomp for sample transportation. M. Caisso is grateful for Ph.D. fellowship funding by the CEA PACFA program.

REFERENCES

(1) McEachern, R. J.; Taylor, P. *J. Nucl. Mater.* **1998**, *254* (2–3), 87–121.
(2) Gras, J.-M.; Quang, R. D.; Masson, H.; Lieven, T.; Ferry, C.; Poinssot, C.; Debes, M.; Delbecq, J.-M. *J. Nucl. Mater.* **2007**, *362* (2–3), 383–394.
(3) Ferry, C.; Poinssot, C.; Cappelaere, C.; Desgranges, L.; Jegou, C.; Miserque, F.; Piron, J. P.; Roudil, D.; Gras, J. M. *J. Nucl. Mater.* **2006**, *352* (1–3), 246–253.
(4) Thomas, L. E.; Einziger, R. E.; Buchanan, H. C. *J. Nucl. Mater.* **1993**, *201*, 310–319.
(5) Warin, D. *J. Nucl. Sci. Technol.* **2007**, *44* (3), 410–414.
(6) Delahaye, T.; Lebreton, F.; Horlait, D.; Herlet, N.; Dehaudt, P. *J. Nucl. Mater.* **2013**, *432* (1–3), 305–312.
(7) Bejaoui, S. In *Proceedings of GLOBAL 2011*; Makuhari, Japan, 2011.
(8) Haas, D. *MOX fuel fabrication experience at Belgonucleaire*; Technical committee meeting on recycling of plutonium and uranium in water reactor fuel; International Atomic Energy Agency: Vienna (Austria), 1997.
(9) Baron, D. D.; Hallstadius, L. In *Comprehensive Nuclear Materials*; Konings, R. J. M., Ed.; Elsevier: Oxford, 2012; pp 481–514.
(10) Andresen, A. F. *Acta Crystallogr.* **1958**, *11* (9), 612–614.
(11) Ball, R. G. J.; Dickens, P. G. *J. Mater. Chem.* **1991**, *1* (1), 105–112.
(12) Loopstra, B. O. *Acta Crystallogr.* **1964**, *17* (6), 651–654.
(13) Wen, X.-D.; Martin, R. L.; Scuseria, G. E.; Rudin, S. P.; Batista, E. R.; Burrell, A. K. *J. Phys. Condens. Matter* **2013**, *25* (2), 25501.
(14) Loopstra, B. O. *J. Appl. Crystallogr.* **1970**, *3* (2), 94–96.
(15) Ackermann, R. J.; Chang, A. T.; Sorrell, C. A. *J. Inorg. Nucl. Chem.* **1977**, *39* (1), 75–85.
(16) Loopstra, B. O. *Acta Crystallogr. B* **1970**, *26* (5), 656–657.
(17) Desgranges, L.; Palancher, H.; Gamaléri, M.; Micha, J. S.; Optasanu, V.; Raceanu, L.; Montesin, T.; Creton, N. *J. Nucl. Mater.* **2010**, *402* (2–3), 167–172.
(18) Benedict, U. *J. Nucl. Mater.* **1970**, *35* (3), 356–361.
(19) Finch, R. J.; Jeremy Kropf, A. *MRS Online Proc. Libr.* **2002**, *757*, null-null.
(20) Remy, E. Étude de la synthèse de sphères d'oxyde d'actinides et/ou de lanthanides et de leur aptitude à la céramisation, Université de Montpellier 2, 2013.
(21) Remy, E.; Picart, S.; Delahaye, T.; Jobelin, I.; Dugne, O.; Bisel, I.; Blanchart, P.; Ayral, A. *J. Nucl. Mater.* **2014**, *448* (1–3), 80–86.

(22) Remy, E.; Picart, S.; Delahaye, T.; Jobelin, I.; Lebreton, F.; Horlait, D.; Bisel, I.; Blanchart, P.; Ayral, A. *J. Nucl. Mater.* **2014**, *453* (1–3), 214–219.
(23) Caisso, M.; Picart, S.; Belin, R. C.; Lebreton, F.; Martin, P. M.; Dardenne, K.; Rothe, J.; Neuville, D. R.; Delahaye, T.; Ayral, A. *Dalton Trans.* **2015**, *44* (14), 6391–6399.
(24) Carjaval, J. R. *Satell. Meet. Powder Diffr. XV IUCr Congr.* **1990**.
(25) Rodríguez-Carvajal, J. *Phys. B Condens. Matter* **1993**, *192* (1–2), 55–69.
(26) Le Bail, A. *Powder Diffr.* **2005**, *20* (4), 316–326.
(27) Newville, M. *J. Synchrotron Radiat.* **2001**, *8* (2), 322–324.
(28) Ravel, B.; Newville, M. *J. Synchrotron Radiat.* **2005**, *12* (4), 537–541.
(29) Rehr, J. J.; Kas, J. J.; Vila, F. D.; Prange, M. P.; Jorissen, K. *Phys. Chem. Chem. Phys. PCCP* **2010**, *12* (21), 5503–5513.
(30) Arab-Chapelet, B.; Martin, P.; Costenoble, S.; Delahaye, T.; Scheinost, A. C.; Grandjean, S.; Abraham, F. *Dalton Trans.* **2016**.
(31) Hoekstra, H. R.; Siegel, S.; Fuchs, L. H.; Katz, J. J. *J. Phys. Chem.* **1955**, *59* (2), 136–138.
(32) Siegel, S.; Hoekstra, H. R. *Inorg. Nucl. Chem. Lett.* **1971**, *7* (6), 497–504.
(33) Greaves, C.; Fender, B. E. F. *Acta Crystallogr. B* **1972**, *28* (12), 3609–3614.
(34) Kvashnina, K. O.; Butorin, S. M.; Martin, P.; Glatzel, P. *Phys. Rev. Lett.* **2013**, *111* (25), 253002.
(35) Shannon, R. D. *Acta Crystallogr. Sect. A* **1976**, *32* (5), 751–767.
(36) Jones, L. H. *Spectrochim. Acta* **1959**, *15*, 409–411.

For table of contents only.

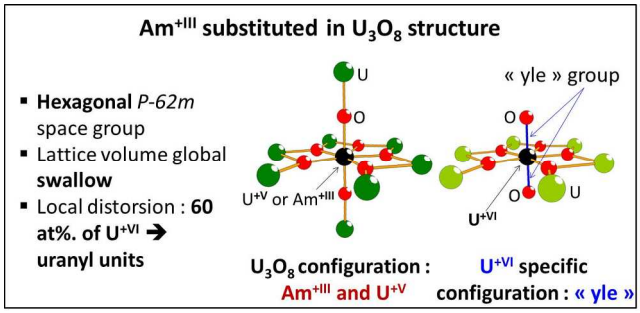


This paper presents first assumption for trivalent Am substitution in $U_3O_8$ structure. Structural properties of this unknown mixed oxide are presented for first time through combination of XRD, XANES and EXAFS measurements.